The EMBO Journal (2011) 30, 2532–2544 | © 2011 European Molecular Biology Organization | All Rights Reserved 0261-4189/11
www.embojournal.org

THE EMBO JOURNAL

Nephrocystins and MKS proteins interact with IFT particle and facilitate transport of selected ciliary cargos

Chengtian Zhao and Jarema Malicki*

Division of Craniofacial and Molecular Genetics, and Program in Genetics, Sackler School of Graduate Biomedical Studies, Tufts University, Boston, MA, USA

Cilia are required for the development and function of many organs. Efficient transport of protein cargo along ciliary axoneme is necessary to sustain these processes. Despite its importance, the mode of interaction between the intraflagellar ciliary transport (IFT) mechanism and its cargo proteins remains poorly understood. Our studies demonstrate that IFT particle components, and a Meckel–Gruber syndrome 1 (MKS1)-related, B9 domain protein, B9d2, bind each other and contribute to the ciliary localization of Inversin (Nephrocystin 2). B9d2, Inversin, and Nephrocystin 5 support, in turn, the transport of a cargo protein, Opsin, but not another photoreceptor ciliary transmembrane protein, Peripherin. Interestingly, the components of this mechanism also contribute to the formation of planar cell polarity in mechanosensory epithelia. These studies reveal a molecular mechanism that mediates the transport of selected ciliary cargos and is of fundamental importance for the differentiation and survival of sensory cells.

The EMBO Journal (2011) **30,** 2532–2544. doi:10.1038/emboj.2011.165; Published online 20 May 2011
Subject Categories: membranes & transport; neuroscience
Keywords: hair cell; photoreceptor; planar cell polarity; sensory neuron; zebrafish

Introduction

Sensory neurons of vertebrates and invertebrates frequently feature well-differentiated cilia that in some cases form specialized detector structures, such as photoreceptor outer segments in the vertebrate eye. Photoreceptors in the eye, hair cells of the auditory system, and olfactory sensory neurons, all feature prominent cilia, which are required for the function of these cells (see, for example, Tsujikawa and Malicki, 2004). The importance of cilia in photoreceptor cells is particularly obvious. The vertebrate photoreceptor utilizes ca. 10^8–10^9 visual pigment molecules, which are synthesized in the cell body and from there transported into the outer segment along the photoreceptor connecting cilium (reviewed in Rodieck, 1973; Pugh and Lamb, 2000; Kennedy and Malicki, 2009). Although in a smaller quantity, olfactory cilia also contain receptors and other elements of the olfactory signal transduction cascade (McEwen *et al*, 2007; Hengl *et al*, 2010). The role of hair cell cilia, kinocilia, in auditory perception is less clear. As cilia are devoid of protein synthesis, the formation of cilliary axoneme and structures that derive from cilia, such as photoreceptor outer segments, requires the translocation of proteins from the cytoplasm. These proteins are thought to be the cargo of a ciliary transport mechanism, referred to as the intraflagellar transport (IFT). Although it is frequently assumed that ciliary transport is mediated by a protein complex, known as the IFT particle (reviewed in Rosenbaum and Witman, 2002; Pedersen and Rosenbaum, 2008; Silverman and Leroux, 2009), the mechanisms that mediate the interaction of the IFT machinery with ciliary 'cargo' proteins remain virtually unknown.

In addition to IFT particle components, which have been described in considerable depth, several other groups of ciliary proteins have been characterized. In contrast to the IFT particle, which has been researched mostly in model organisms, *Chlamydomonas* and *Caenorhabditis elegans*, these proteins were mainly discovered through the studies of human syndromic ciliopathies, and classified based on human phenotypes. The best studied of these proteins are associated with the Bardet–Biedl syndrome (BBS), nephronophthisis (NPHP), and Meckel–Gruber syndrome (MKS) (reviewed in Adams *et al*, 2007). Consistent with the role of ciliary proteins in the differentiation of sensory neurons, human symptoms associated with mutations in these proteins include blindness due to photoreceptor degeneration, anosmia, and in some cases also hearing defects (Adams *et al*, 2007; Jenkins *et al*, 2009). In addition to sensory deficits, mutations in BBS, NPHP, and MKS genes cause polycystic kidney disease, and frequently nervous system defects that range from mental retardation to severe developmental abnormalities, such as encephalocele (Leitch *et al*, 2008; Weatherbee *et al*, 2009). The phenotype of MKS is particularly severe, and involves perinatal lethality.

Several recent studies have made impressive advances in the understanding of the BBS loci on the molecular level (Nachury *et al*, 2007; Seo *et al*, 2010). The protein products of these genes form complexes, one of which appears to coat cytoplasmic vesicles and direct their trafficking to cilia (Jin *et al*, 2010). The understanding of Nephrocystin and MKS protein function is far less advanced. The structures of these proteins are very diverse, and include motifs suggestive of protein–protein interactions, catalytic activity, and membrane association (Hildebrandt *et al*, 2009; Salomon *et al*, 2009; Valente *et al*, 2010). Within each of these two groups, proteins appear to interact physically with each other, although it is not clear whether they form large complexes, similar to the BBS-ome (Olbrich *et al*, 2003; Otto *et al*, 2003;

*Corresponding author. Division of Craniofacial and Molecular Genetics, and Program in Genetics, Sackler School of Graduate Biomedical Studies, Tufts University, 136 Harrison Avenue, M&V Building, Room # 822, Boston, MA 02111, USA. Tel.: +1 617 636 0970; Fax: +1 617 636 2974; E-mail: jarema.malicki@tufts.edu

Received: 12 October 2010; accepted: 19 April 2011; published online: 20 May 2011

Mollet *et al*, 2005; Williams *et al*, 2008; Bialas *et al*, 2009). Likewise, it is not clear how these proteins interact with ciliary transport machinery.

The structural diversity of NPHP and MKS proteins is paralleled by the variety of functions in which they appear to be involved. One of the best-studied Nephrocystin genes, *inversin* (*nephrocystin 2*), encodes a protein containing N-terminal ankyrin repeats and two IQ motifs (Morgan *et al*, 2002b). It localizes to cilia, basal bodies, the mitotic spindle, as well as cell junctions, and forms a complex with N-cadherin (Morgan *et al*, 2002a; Nurnberger *et al*, 2002). The *inversin* mutants feature phenotypes typically associated with cilia defects, such as situs inversus, kidney abnormalities, and photoreceptor degeneration (Morgan *et al*, 1998; O'Toole *et al*, 2006). *Inversin* is also homologous to *diego*, a key regulator of planar cell polarity (PCP) in the fly. Similar to its fly counterpart, the vertebrate Inversin binds two other core PCP proteins: Prickle and Van Gogh (Simons *et al*, 2005). In agreement with these findings, Inversin, and Van Gogh function in convergent extension, a vertebrate model of PCP (Jessen *et al*, 2002; Simons *et al*, 2005). Molecular mechanisms that mediate the involvement of Inversin in such a variety of developmental and physiological processes are yet to be elucidated.

To gain insight into the function of Nephrocystins and MKS proteins, we proceeded to search for binding partners of these polypeptides and test their role via genetic approaches in zebrafish. Our studies reveal direct binding interactions that link Nephrocystins, MKS-like proteins, and the IFT particle. These interactions involve Inversin; an MKS1-related B9 domain protein, B9d2; the Fleer/Dyf-1 polypeptide, and at least one other IFT particle constituent. Both Fleer and B9d2 are involved in localizing Inversin to cilia, and appear to contribute to Van Gogh function in regulating the planar polarity of mechanosensory epithelia. Importantly, B9d2, Inversin, and Nephrocystin 5, are necessary for the efficient transport of a well-studied ciliary cargo protein, opsin. These results indicate that at least some MKS-like proteins and Nephrocystins facilitate the function of the IFT most likely by mediating the interactions of the IFT particle with its cargo. As the ciliary cargo is inherently diverse, this role is consistent with the diversity of cellular and developmental processes that Nephrocystins and MKS proteins are involved in.

Results

An IFT particle component, Fleer, binds MKS1-related protein, B9d2

To gain insight into the interactions of the IFT particle with cargo proteins, we chose to study one of IFT particle components, encoded by the *fleer/dyf-1* gene (Ou *et al*, 2005; Pathak *et al*, 2007). *fleer/dyf-1* mutations are thought to affect the function of the Osm-3 kinesin and tubulin-tyrosine ligase-like proteins (Ou *et al*, 2005; Pathak *et al*, 2007). Although these findings suggest that the Fleer protein may mediate the interaction of the IFT particle with cargo molecules, its binding partners remain unknown. We therefore proceeded to search for Fleer interaction partners via a yeast two-hybrid screen. Screening of ca. 1.1 mln colonies with the full-length Fleer as a bait identified two potential interaction partners: an IFT particle component, Ift74, and the B9d2 protein. B9d2 is very well conserved in evolution (Supplementary Figure S1) and shares homology (the so-called B9 domain) with MKS1, a protein defective in a human cilia-related disorder known as MKS. MKS1 and B9d2 appear to be closely functionally related: they display similar subcellular localization patterns, a downregulation of their function in mammalian cells results in cilia defects, they both interact genetically with nematode Nephrocystins, and, finally, their subcellular localizations in *C. elegans* are interdependent (Town *et al*, 2008; Williams *et al*, 2008; Bialas *et al*, 2009).

Further studies of Fleer–B9d2 binding using yeast two-hybrid tests of human proteins revealed that B9d2 interacts with the N-terminal region of Fleer (Figure 1A and data not shown), and a reciprocal experiment demonstrated that the C-terminal amino acids 107–175 of B9d2 are both necessary and sufficient to mediate its interaction with Fleer (Figure 1B). In agreement with these findings, GST-B9d2 fusion pulls down MBP-Fleer but not MBP alone (Figure 1C). These data demonstrate that Fleer and B9d2 bind each other.

The same yeast two-hybrid screen that identified B9d2 as a binding partner of Fleer, also revealed an IFT particle component, Ift74. A dissection of this binding interaction using yeast two-hybrid assay revealed that the same N-terminal Fleer fragment that interacts with B9d2 is sufficient to bind Ift74. In a reciprocal yeast two-hybrid experiment, we determined that the C-terminal amino acids 352–600 of Ift74 are sufficient to mediate its interaction with Fleer (data not shown). The full-length Ift74 interacted only weakly with Fleer, however. As these results suggested that Fleer binds the IFT particle, we asked whether it also interacts with other IFT particle components. Taking advantage of yeast two-hybrid constructs generated in previous studies (Baker *et al*, 2003), we tested Ift88, Ift20, Ift52, and an N-terminal fragment of Ift57 for interactions with Fleer. Only Ift52 bound to Fleer in this assay (Figure 1D). Additional yeast two-hybrid tests revealed that, again, the N-terminal Fleer fragment of 364 amino acids is both necessary and sufficient to mediate this interaction (Figure 1D), and a reciprocal yeast two-hybrid experiment demonstrated that the C-terminal amino acids 219–426 of Ift52 are both necessary and sufficient to bind Fleer (Figure 1E). To confirm these findings, we performed pull-down experiments, and found that GST-Ift52 binds MBP-Fleer but not MBP alone (Figure 1F). Yeast two-hybrid tests of the Fleer N-terminus against 10 other polypeptides did not reveal binding interactions, arguing against the possibility that this region of the Fleer polypeptide tends to interact nonspecifically with other proteins (Supplementary Figure S2). These results, along with data published by others (Fan *et al*, 2010), indicate that Fleer binds the IFT particle, via the interaction with Ift52, and possibly also other IFT polypeptides.

b9d2 functions in ciliogenesis

As zebrafish *fleer* (*flr*) mutants display a clear loss of cilia (Doerre and Malicki, 2002; Pathak *et al*, 2007) (Supplementary Figure S3), and our data indicate that Fleer and B9d2 bind each other, we asked whether *b9d2* functions in ciliogenesis. Treatments with high doses of two different anti-*b9d2* morpholinos did not, however, produce kidney cysts, and resulted in only a low frequency of curly body axis, a phenotype characteristic of cilia defects (data not shown) (Tsujikawa and Malicki, 2004; Zhao and Malicki, 2007; Omori *et al*, 2008). Likewise, we did not observe obvious changes in the length of morphant cilia. In contrast to the absence of changes in cilia

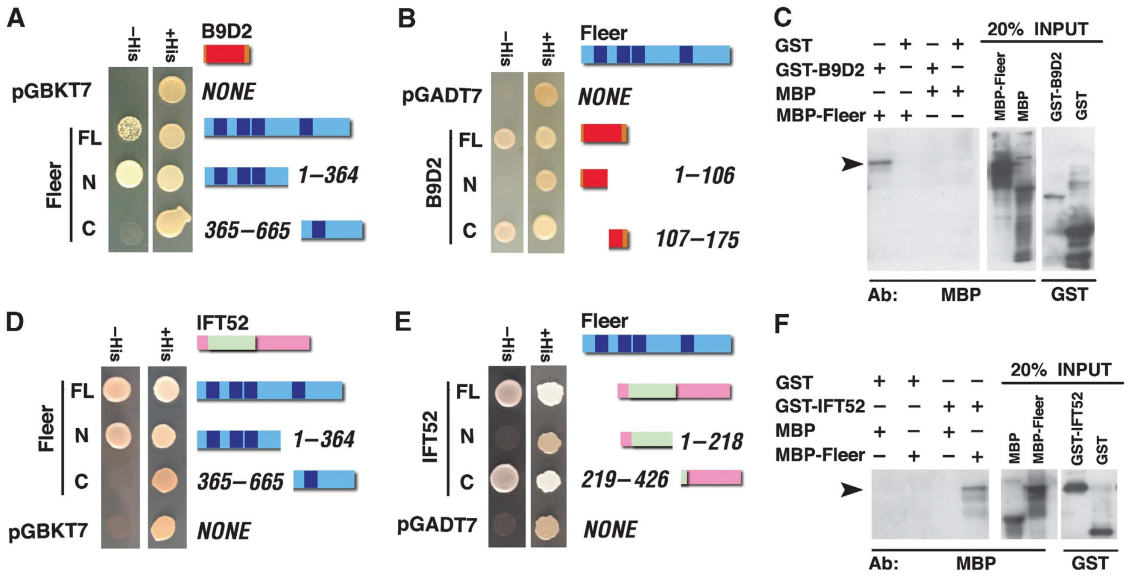

Figure 1 Fleer binds Ift52 and B9d2. (**A**) Yeast two-hybrid tests for binding between full-length human B9d2 and human Fleer (TTC30B) fragments. B9D2 binds the N-terminal region of Fleer. (**B**) Yeast two-hybrid test for the binding of full-length Fleer to B9d2 and its fragments. Fleer binds the C-terminal region of B9D2. (**C**) Pull down of MBP-Fleer using a GST-B9d2 fusion. Western blots with anti-MBP and anti-GST antibodies are shown. (**D**) Yeast two-hybrid test for binding between mouse full-length Ift52 and human Fleer. Ift52 binds the N-terminal portion of Fleer. (**E**) Yeast two-hybrid tests for binding between full-length Fleer and Ift52. Fleer binds the C-terminal portion of Ift52. (**F**) Pull down of MBP-Fleer using GST-Ift52 (full-length) fusion. Western blot as in (**C**). In all yeast two-hybrid assays shown, Fleer was used as a bait. (**A**, **B**, **D**, **E**) Fleer is depicted as blue horizontal bars, Ift52 and B9d2 as pink and orange bars, respectively. TPR repeats, the GIFT domain, and the B9 domain are indicated in dark blue, pale green, and red, respectively. Arrowheads in (**C**, **F**) indicate the pull-down product.

morphology, *b9d2* knockdown affects opsin localization in photoreceptor cells (Figure 2A and B). To show that knockdown is effective, we used a reporter construct. Both ATG- and 5′ UTR-targeted morpholino reduced reporter expression to background level (Figure 2C). As the lack of cilia length phenotype contrasts with mouse data (Town *et al*, 2008), we asked whether a double knockdown of *b9d2* and *fleer* affects ciliogenesis. This, indeed, turned out to be the case: while a low dose of anti-*fleer* morpholino does not produce a shortening of cilia, the same dose combined with an anti-*b9d2* morpholino results in a shortening of neural tube and nasal cilia (Figure 2D–F; Supplementary Figure S4A). Cilia length changes were not accompanied by obvious differences in tubulin glutamylation as detected with the GT335 antibody (Supplementary Figure S4B). Knockdown of *b9d2* function in *flr*^{m477} mutant heterozygotes also resulted in a shortening of cilia (Supplementary Figure S4C), confirming the results of double morphant analysis. Consistent with this ciliary phenotype, we found that GFP-B9d2 fusion protein localizes to cilia (Figure 2G; Supplementary Figure S4D). These results indicate that in agreement with binding studies, *b9d2* and *fleer* function in concert during ciliogenesis.

The absence of strong external phenotype and cilia length changes in *b9d2* knockdown animals may be due to redundancy with two other B9 domain proteins, B9d1 and Mks1, which are functionally related to B9d2 (Williams *et al*, 2008; Bialas *et al*, 2009). To test whether this is the case, we performed double and triple knockdowns of all three B9 domain proteins in all combinations. Based on RT–PCR analysis of transcripts, knockdowns of *b9d1* and *mks1* eliminated the function of these genes completely or nearly completely (Supplementary Figure S5A and B). None of these knockdowns, however, produced a shortening of cilia length in the kidney or the spinal cord at 24 h.p.f. (Supplementary Figure S5C and data not shown), possibly due to the presence of maternal contribution. We did, however, observe a synergistic increase in the frequency of hydrocephalus in the triple knockdown, compared with single knockdowns, indicating that these loci interact genetically (Supplementary Figure S5D).

B9d2 binds a Nephrocystin, Inversin

The nematode *b9d2* homologue was reported to interact genetically with *nephrocystins* 1 and 4 (Williams *et al*, 2008). To investigate whether B9d2 physically interacts with Nephrocystins, we tested human Nephrocystins 1 through 5 for binding to human B9D2 using yeast two-hybrid assay, and found that only one, Inversin (Nephrocystin 2), binds B9d2 (Figure 3A). Further dissection of Inversin and B9D2 polypeptides revealed that the N-terminal fragment of 553 amino acids of Inversin is both necessary and sufficient to bind B9D2 (Figure 3C), and the amino acids 107–175 of B9D2 are both necessary and sufficient to mediate B9D2 binding to Inversin (Figure 3D). In agreement with these data, we found that GST-B9D2 binds Inversin-MBP but not MBP alone (Figure 3B). To identify additional interactions, we tested B9D2 and Inversin for binding to the same panel of IFT particle components that we studied for interactions with the Fleer protein above, and found that B9D2 also binds IFT88 (data not shown). In contrast to that, Inversin does not consistently bind any of the IFT proteins tested in this assay. These analyses strongly suggest that Inversin interacts with the IFT particle via binding the B9d2 protein. It is worth to point out that the binding of Inversin to B9D2, an MKS1-related protein, is in agreement with reports that *situs inversus* is associated with mutations in both human Inversin and MKS1 but not with defects in other nephrocystins or in MKS3 (Khaddour *et al*, 2007; Hildebrandt *et al*, 2009).

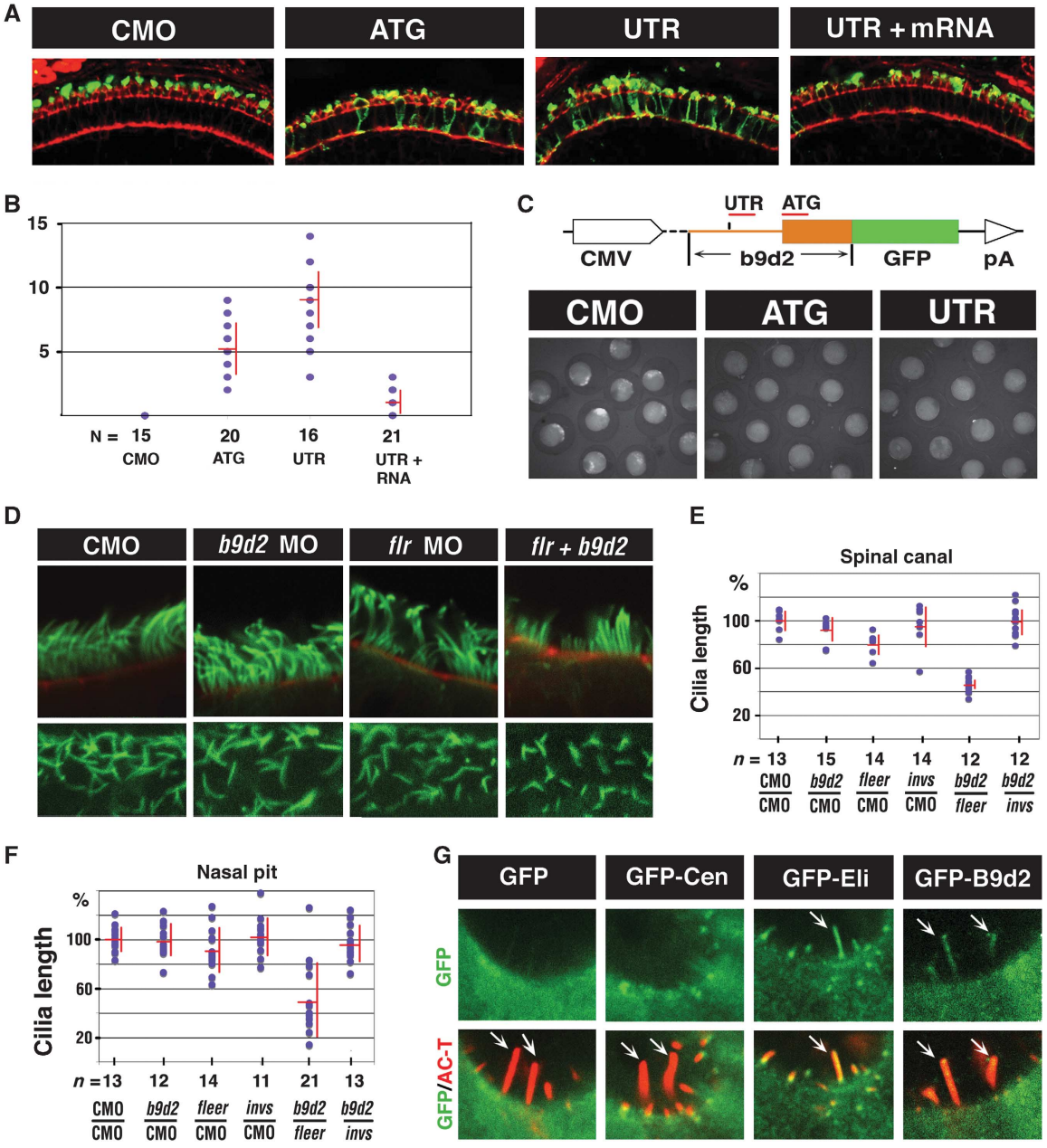

Figure 2 *b9d2* functions in ciliogenesis. (**A**) Confocal images of cryosections through the photoreceptor cell layer of control and *b9d2* morphant animals as indicated. Sections were stained with anti-opsin antibody (in green) and counterstained with phalloidin (in red). (**B**) Frequency of opsin mislocalization in control animals, morphants, and mRNA rescued morphants as indicated. Shown is the number of photoreceptor cells that feature opsin mislocalization per an arbitrary unit of length as measured on transverse cryosections through the retina. *n*, the number of embryos. (**C**) Schematic representation of the GFP reporter construct used to evaluate *b9d2* knockdown efficiency. The UTR morpholino is targeted to the position (−56) of the 5′ UTR. Images below show GFP expression in control and morphant animals. (**D**) Confocal images of cilia in the nasal pit (upper row) and the spinal canal (lower row) visualized with anti-acetylated-α-tubulin antibody (green) in whole zebrafish embryos. Animals were treated with morpholino oligonucleotides as indicated. In upper panels, embryos were counterstained with Alexa-546 phalloidin (red). (**E**, **F**) Cilia length distribution in the spinal canal (**E**) and the nasal pit (**F**) of morphants and control animals as indicated below each graph. Each dot represents an average of 5 (for nose) and ⩾10 (for spinal cord) measurements from a single embryo. Red horizontal and vertical bars show average and s.d., respectively. *n*, the number of embryos inspected. The vertical axis shows the length of cilia as the percentage of the average wild-type length. 100% equals 4.3 μm in (**E**) and 8.3 μm in (**F**). In both (**E**, **F**), $P<0.0001$ for *b9d2/fleer* double knockdown, compared with single knockdowns. (**G**) Confocal images of hair cells expressing GFP, GFP-centrin (GFP-Cen), GFP-Elipsa (GFP-Eli), or GFP-B9d2. Embryos were double stained for acetylated tubulin to visualize cilia (in red, arrows) and for GFP (in green). Upper panels show GFP signal alone. Overlays of green and red signal are shown in lower panels. In (**A**, **D**, upper panels, and **G**), apical is up. (**D**, lower panels) show face view of ciliated epithelium. CMO, control morpholino.

Nephrocystins, Inversin and NPHP5, together with MKS1-related proteins facilitate the transport of ciliary cargo

What is the role of Inversin in cilia? Inversin loss of function does not cause morphological or ultrastructural defects in cilia, indicating that it is unlikely to mediate the transport of structural ciliary proteins, such as tubulins (Otto *et al*, 2003; Watanabe *et al*, 2003; Phillips *et al*, 2004). In agreement with that, cilia retain normal length in *inversin/b9d2* double knockdowns (Figure 2E and F). Although it is unlikely to have a role in the transport of proteins that form the ciliary axoneme, Inversin and other Nephrocystins may contribute

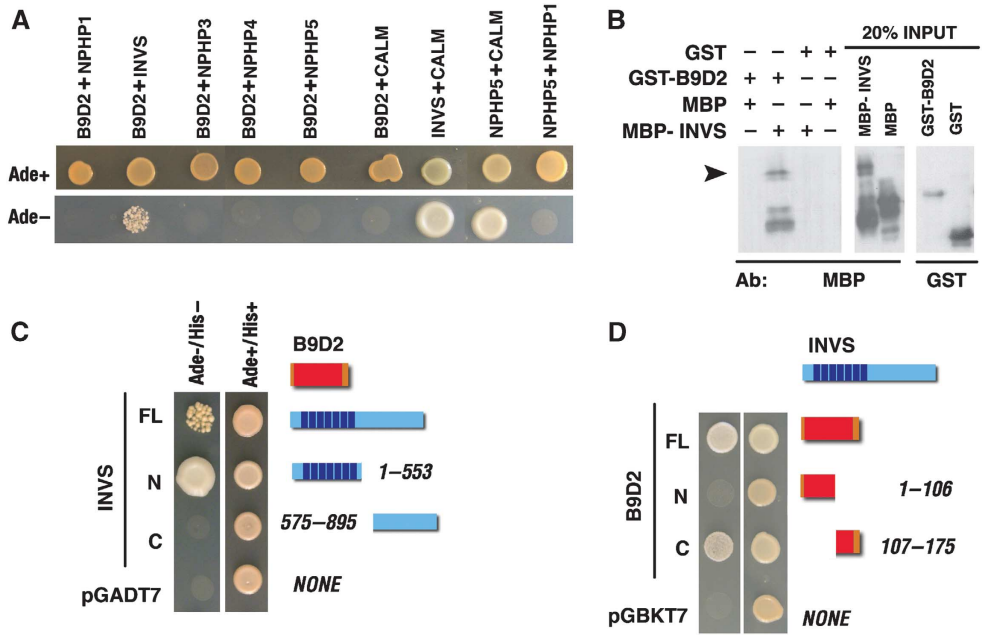

Figure 3 B9D2 binds to Inversin/NPHP2. (**A**) Yeast two-hybrid tests for binding between human B9D2 and five human Nephrocystins (NPHP1–5). Binding of Inversin and NPHP5 to Calmodulin are included as positive controls. NPHP5/NPHP1 interaction is provided as a negative control. B9D2 binds Inversin but not other Nephrocystins tested. (**B**) Pull down of MBP-Inversin using GST-B9D2 fusion. Western blot stained with anti-MBP or anti-GST antibodies, as indicated. Arrowhead indicates the pull-down product. (**C**) Yeast two-hybrid tests for binding between full-length B9D2 and Inversin fragments. B9D2 binds the N-terminal ankyrin repeat region of Inversin. (**D**) The results of yeast two-hybrid tests for interactions between full-length Inversin and B9D2 fragments. Inversin binds the C-terminal region of B9D2. In (**C**, **D**) Inversin and B9D2 are depicted as blue and orange horizontal bars, respectively. Vertical dark blue stripes denote ankyrin repeats. The B9 domain is indicated in red.

to the transport of nonstructural ciliary cargo molecules, such as transmembrane receptors. To test this possibility, we decided to analyse the transport of opsin, one of the best-studied potential cargo molecules of the IFT (Tam *et al*, 2000).

Traditionally, ciliary transport defects in the photoreceptor cell are detected in mutants as protein accumulation in the cell body (Figure 6C–E) (Marszalek *et al*, 2000; Zhao *et al*, 2003). It is not clear, however, whether such phenotypes are due to a defective transport or to aberrations of photoreceptor structure, such as the breakdown of a diffusion barrier between the inner and outer segments. To circumvent this difficulty, we fused GFP to 44 C-terminal amino acids of opsin, a sequence sufficient for outer segment targeting (Tam *et al*, 2000). When transiently expressed in genetically normal photoreceptors from a heat-shock promoter, this fusion protein is transported into the outer segment, and is nearly completely absent in the inner segment within 4 h (Figure 4A and B). In contrast to that, following the knockdown of *inversin*, *b9d2*, or another nephrocystin, *nphp5*, GFP-opsin persists in the inner segment at a high level for at least 9 h. It is eventually cleared from the inner segment by 24 h after heat shock (Figure 4A and B). As this phenotype involves a delay of GFP-opsin transport and not a permanent mislocalization, it is less likely to result from a structural damage to the outer segment. These results support the conclusion that Nephrocystins and MKS proteins facilitate the transport of nonstructural ciliary cargo proteins.

One possible reason for the delay of opsin clearance from the photoreceptor cell body is a slow down of its degradation in the inner segment of morphant animals. To investigate this possibility, we monitored GFP-opsin degradation in *oval/ift88* mutants. These animals lack outer segments entirely, and so opsin is not transported from the cell body (Tsujikawa and Malicki, 2004). In *oval/ift88* mutant background, the rate of opsin degradation is the same for morphant and control animals (Figure 4D; Supplementary Figure S6C). These data demonstrate that a decrease in the inner segment degradation rate does not account for a delay of opsin transport in *invs*, and *b9d2* morphants. Taken together, the above results indicate that two nephrocystins, *inversin* and *nphp5*, as well as an MKS1-related gene, *b9d2*, are necessary to maintain the normal rate of opsin transport into the outer segment.

The transport of Peripherin/Rds, another outer segment transmembrane protein, is mediated by a localization signal different from the one identified in opsin (Tam *et al*, 2004). To test whether Peripherin/Rds is another ciliary cargo that requires Nephrocystin function, we monitored the transport of Peripherin-GFP fusion using the same assay as for opsin. This fusion polypeptide is not affected following the knockdowns of *inversin*, and *b9d2* (Figure 4A and C; Supplementary Figure S6A). Rds-GFP also continues to localize to the outer segment even when *nphp5* function is completely or nearly completely absent (Supplementary Figure S6A and B). Finally, we have not observed Rds-GFP mislocalization in partial knockdowns of *ift88*, and *ift20*, although opsin transport is impaired in these conditions (data not shown). These results indicate that peripherin and opsin rely on different ciliary transport mechanisms.

B9d2 and an IFT protein, Fleer, localize Inversin to the ciliary compartment

What is the function of binding between Inversin, B9d2, and the IFT particle? One obvious possibility is that these interactions localize Inversin to the ciliary compartment. To test this idea, we overexpressed an Inversin-GFP fusion polypeptide in auditory hair cells, and measured GFP signal intensity

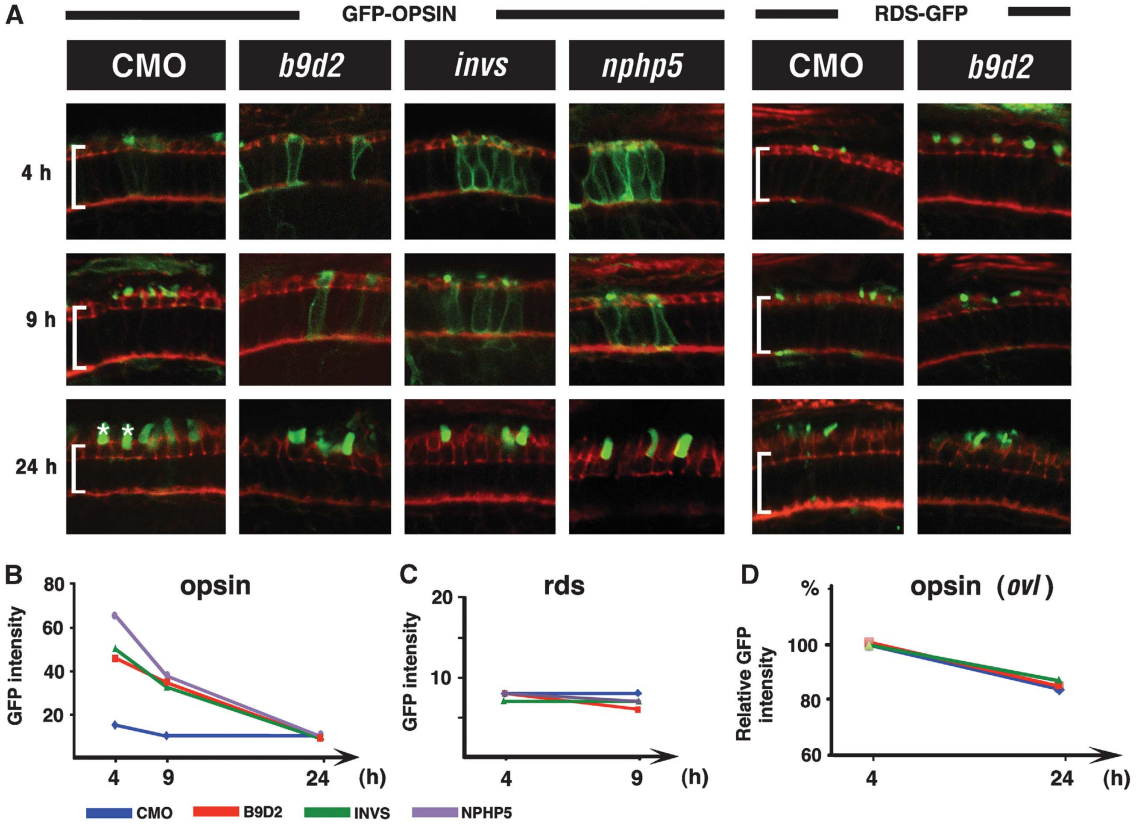

Figure 4 *b9d2* and *nephrocystins* function in ciliary trafficking of opsin. (**A**) Confocal images of transverse sections through retinae of animals treated with morpholinos against *b9d2*, *invs*, and *nphp5*, as indicated. The subcellular localization of GFP-Rhodopsin (left) or Peripherin/RDS-GFP (right) is shown 4, 9, and 24 h after a heat shock (in green). Sections are counterstained with phalloidin (in red). Each row represents a different time point after heat shock as indicated to the left. Brackets indicate photoreceptor cell bodies; asterisks, outer segments. (**B**) Graph of GFP-Rhodopsin signal intensity in the photoreceptor cell bodies of morpholino-treated embryos. (**C**) Graph of Peripherin-GFP signal intensity in the photoreceptor cell bodies of morpholino-treated embryos. (**D**) Graph of GFP-Rhodopsin signal intensity in photoreceptor cell bodies of morpholino-treated *oval/ift88* mutants. Percentage change relative to signal intensity at 4 h after heat shock is shown. Intensity at 4 h equals 100%. (**B–D**) Each colour line corresponds to a treatment with a different morpholino as shown in the legend below. The *y* axis indicates GFP signal intensity, *x* axis is the time after heat shock. Note that the scale on *y* axis varies. CMO, control morpholino; NPHP5, Nephrocystin 5; INVS, inversin.

in the cilia of *b9d2* and control knockdown animals relative to the cell body (Figure 5A and B). We found that the level of Inversin-GFP in cilia is reduced in *b9d2* morphants, compared with control morpholino-treated embryos (Figure 5B; $P<0.001$, three independent experiments using 5 μg/μl of morpholino). In contrast to that, the same treatment does not affect the ciliary localization of an IFT particle component, Elipsa (Figure 5B). These results indicate that in agreement with the predictions of our binding studies, B9d2 facilitates the localization of Inversin to cilia.

To analyse Inversin localization further, we investigated whether *fleer* is required to localize it to the ciliary shaft. As the complete absence of *fleer* function eliminates cilia (Supplementary Figure S3), we performed partial knockdowns with a low dose of anti-*fleer* morpholino. A double knockdown with low doses of anti-*fleer* and anti-*b9d2* morpholinos (2 μg/μl each) produces a sharp decrease in Inversin-GFP signal, to ca. 10% of the control value, while the same concentration of either morpholino alone has a much weaker effect (Figure 5C; Supplementary Figure S7). Importantly, the length of the ciliary shaft is not affected in these experiments (Figure 5D). These results indicate that *b9d2* and *fleer* function to either localize or stabilize Inversin in the ciliary compartment, and are in agreement with the model in which B9d2 and Fleer provide a link between the IFT particle and Inversin (Figure 8).

The results of binding tests suggest that Inversin, B9d2, and Fleer form a complex. To test this possibility further, we appended these proteins with unique tags and mixed them in a single binding reaction. In a pull-down experiment that followed, MBP-Inversin co-purified with His-Fleer in the presence of GST-B9d2, but not in the presence of GST alone (Figure 5E). The presence of the Fleer polypeptide in the pull-down product was confirmed by mass spectrometry (data not shown). This result indicates that at least *in vitro* B9d2 is required to mediate the binding of Inversin to Fleer, and that a Nephrocystin (Inversin), an MKS protein (B9D2), and an IFT component (Fleer) form a single complex.

Inversin, b9d2, and IFT loci interact genetically in many cilia-related processes

Our binding studies imply that Inversin, B9d2, Fleer, and Ift52 proteins function in the same pathway. If so, the corresponding loci should interact genetically. To test whether this is the case, we injected embryos with combinations of morpholinos targeted to these genes. The dose of each morpholino was adjusted so that injections of single morpholinos did not produce a phenotype or resulted in a weak phenotype only. Three cilia-related phenotypes were studied in morphant animals: body axis curvature, left–right asymmetry, and opsin localization.

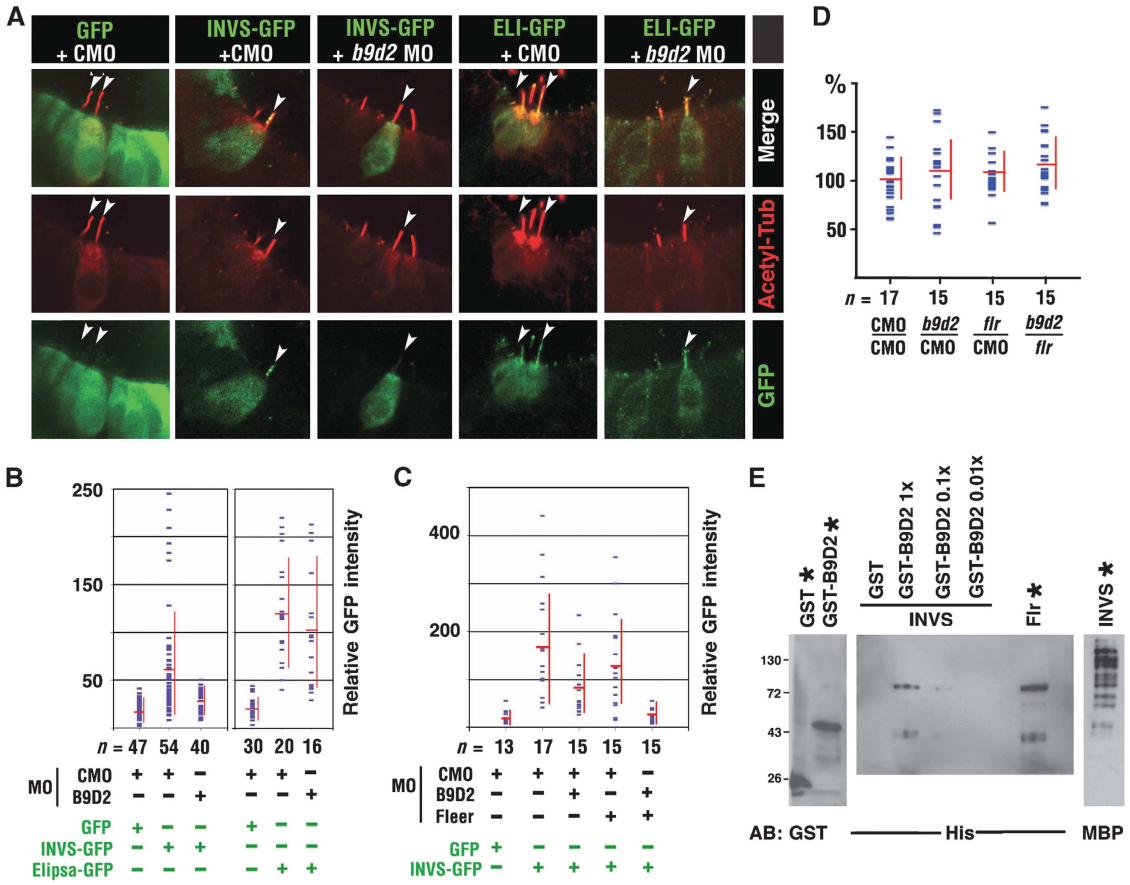

Figure 5 *b9d2* and *fleer* contribute to the ciliary localization of Inversin. (**A**) Confocal images of hair cells expressing GFP, Inversin-GFP (INVS-GFP), or Elipsa-GFP (ELI-GFP), in embryos treated with either a control (CMO) or with anti-*b9d2* morpholino (*b9d2* MO) as indicated. Cilia are visualized via anti-acetylated-α-tubulin immunostaining (in red). Red and green channels as well as a merged image of both are provided in separate rows. (**B**) Quantitation of the GFP signal in the kinocilia of hair cells expressing GFP, Inversin-GFP, or Elipsa-GFP, in animals treated with control or anti-*b9d2* morpholino. The intensity of GFP signal was averaged along the length of ciliary axoneme. To compensate for expression level variation in different cells, shown is the ratio of signal intensities in the ciliary axoneme and the cell body. *n*, the number of cells analysed. (**C**) Quantitation of GFP or Inversin-GFP signal in hair cell kinocilia of control, *b9d2* and *fleer* single morphants, as well as *b9d2/fleer* double morphants. (**D**) Cilia length (percentage of the average control value) in embryos treated with morpholino oligonucleotides as indicated. 100% equals 8.0 μm. Measurements performed on the same images as in (**C**). (**E**) Double pull down of B9d2 and Fleer with MBP-Inversin. MBP-Inversin pulls down His-Flr in the presence of GST-B9d2 but not in the presence of GST alone. For each protein, 20% of input is shown (lanes marked with asterisks). CMO, control morpholino.

A curly shape of the body axis is characteristic of cilia defects in zebrafish (Sun *et al*, 2004; Tsujikawa and Malicki, 2004; Omori *et al*, 2008). We evaluated the frequency of this phenotype in double morphants of *inversin*, *b9d2*, and two IFT particle components, *fleer*, and *ift52* (six combinations total; Figure 6A). Single morpholinos injected together with a control morpholino were used as a reference. We found that the frequency of curly body phenotype in double knockdown embryos is at least twice as high as the sum of frequencies in single gene knockdowns (Figure 6A).

Defects of left–right asymmetry are also characteristic of ciliary malfunction (Morgan *et al*, 1998; Murcia *et al*, 2000). To test our model of protein–protein interactions, we performed double knockdowns of *inversin/b9d2*, *b9d2/fleer*, and *fleer/ift52*, and evaluated left–right asymmetry by studying the expression patterns of *lefty1* and *lefty2*, two genes characterized by expression domains preferentially positioned on the left side of the body axis (Bisgrove *et al*, 1999). In all cases, the frequency of left–right asymmetry defects after double knockdowns was significantly higher than the sum of frequencies detected following knockdowns of single genes (Figure 6B).

As the third test of functional interactions, we studied opsin localization. Knockdowns of single genes, *invs*, *b9d2*, *flr*, or *ift52*, with low doses of antisense morpholinos produce rod opsin mislocalization with the same frequency as control morpholinos (Figure 6C and D; Supplementary Figure S8A and B). In contrast to that, about a half of all photoreceptors accumulate opsin ectopically throughout their bodies in *b9d2/invs*, *flr/invs*, *b9d2/flr*, and *flr/ift52* double knockdown animals when the same concentrations of morpholinos are applied (Figure 6C and D; Supplementary Figure S8A and B; data not shown). Ultrastructural analysis of photoreceptors from *flr/invs* double knockdown animals did not reveal gross morphological malformations, except for a shortening of the outer segment (Supplementary Figure S8D and E). To exclude the possibility that opsin mislocalization in double morphants is a consequence of a delayed morphogenesis, we monitored photoreceptor differentiation by measuring the ratio (n/m) of the apical segment length (n) to the entire

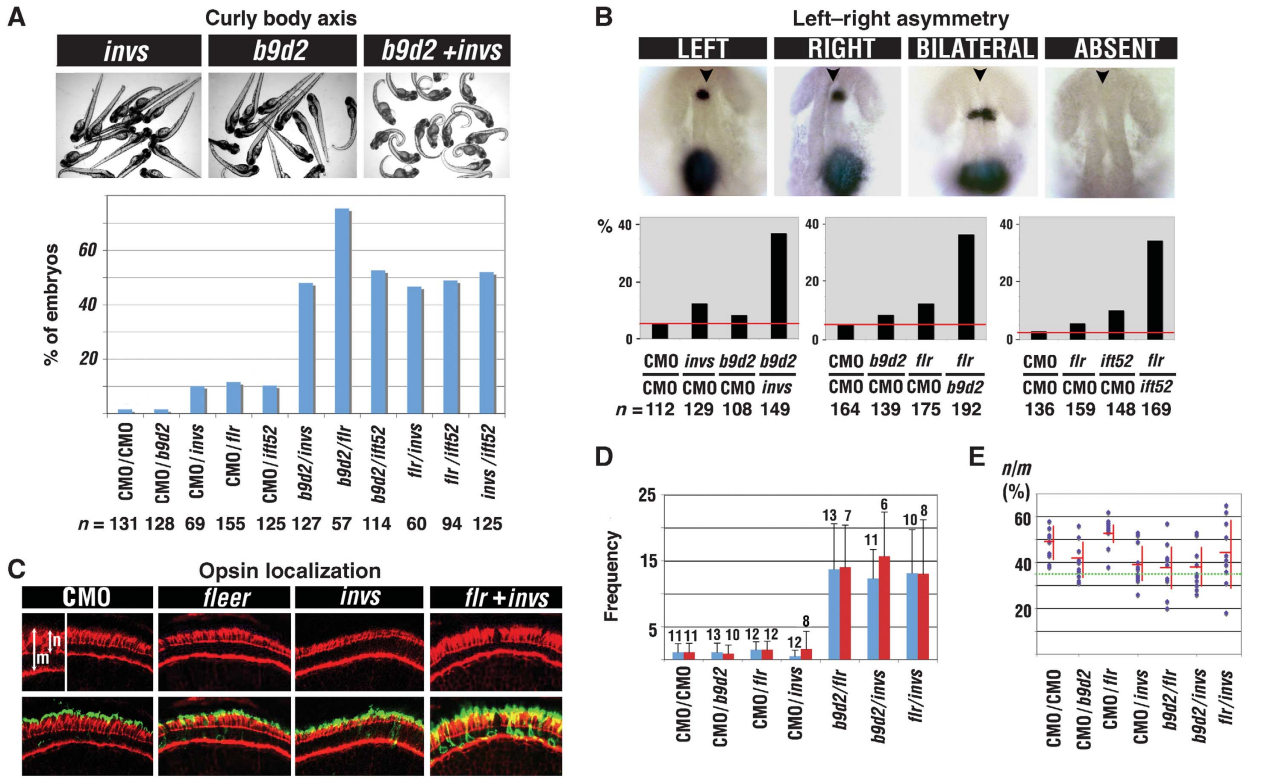

Figure 6 Genetic interactions between *inversin*, *b9d2*, *fleer*, and *ift52*. (**A**) Percent frequencies of curly body axis phenotype in single and double morphants as indicated. Panels above the graph show examples of morpholino-induced phenotype. All six combinations of double knockdowns show dramatically increased frequency of the curly body phenotype, compared with single knockdowns. (**B**) Images of embryos following whole-mount *in situ* hybridization with *lefty1* and *lefty2* probes to asses left–right asymmetry. Shown are examples of four expression patterns found in morpholino-treated embryos. Left, expression confined to the left side of the embryo. Right, expression confined to the right side. Bilateral, expression on both sides. Absent, expression absent. Anterior is up, arrowheads indicate the midline. Graphs below present percent frequencies of left–right asymmetry defects (right, bilateral, or absent expression) in single and double morphants, as indicated. Red horizontal line indicates the baseline level of nonspecific defects in control morpholino-treated animals. (**C**) Confocal images of transverse sections through retinae of animals treated with morpholinos against *flr*, *invs*, and *flr* + *invs*, as indicated. Sections were stained with anti-opsin antibodies (in green), and counterstained with phalloidin (in red). Inset shows an enlarged area from the neighbouring panel. *m*, length of the entire photoreceptor cell. *n*, length of the apical segment of the photoreceptor cell. (**D**) The frequency of opsin mislocalization in single and double morphants, as indicated. Shown is the number of photoreceptor cells that feature opsin mislocalization per retina. Measurements were performed on transverse cryosections through the retina (one per embryo) and normalized for changes in the length of the photoreceptor cell layer. To exclude the possibility that opsin mislocalization is due to a developmental delay, we monitored the n/m ratio. This parameter increases as photoreceptor differentiate. Red bars indicate the frequency of defects in retinae with n/m ratio $\geqslant 35\%$, as indicated in the next panel. (**E**) The ratio of apical segment length (n) to cell length (m) in photoreceptors from the same set of experimental samples as in (**D**). Dashed horizontal line indicates the n/m ratio of 35%. Each dot corresponds to three independent measurements performed on a single section. *n*, number of embryos (provided above bars in **D**). CMO, control morpholino.

photoreceptor cell length (m) as defined in Figure 6C. This ratio increases during photoreceptor differentiation (Omori and Malicki, 2006). Subsequently, we used this ratio to identify cells that are potentially delayed (n/m <35%) and exclude them from statistical analysis (Figure 6E; Supplementary Figure S8C). We found that even retinae of double morphants that feature well-differentiated photoreceptors display a strong synergistic increase in opsin mislocalization, compared with single knockdowns (Figure 6D; Supplementary Figure S8B, red bars). In a control experiment, we also performed a double knockdown of *b9d2* and another ciliary gene involved in photoreceptor degeneration, *bbs4* (Abd-El-Barr *et al*, 2007). We observed only an additive effect in this assay (Supplementary Figure S8F). Similarly, a double knockdown of *b9d2* and *pkd2* did not reveal synergistic interactions (Supplementary Figure S8G), and although *pkd2/invs* double knockdown produced a synergistic phenotype, its frequency was very low (Supplementary Figure S8G). Taken together, the studies of three cilia-related phenotypes: body curvature, left–right asymmetry, and opsin localization, support the conclusions of binding studies that Inversin, B9d2, and IFT particle components display closely related functions.

Inversin, b9d2, and IFT genes contribute to PCP

IFT particle components function in the planar polarity of mechanosensory hair cells (Jones *et al*, 2008). Interestingly, the Vangl (Van Gogh/Strabismus) protein, a core regulator of PCP, has been reported to localize to cilia and to bind Inversin (or its fly homologue, Diego), both in Xenopus and in the fly (Das *et al*, 2004; Ross *et al*, 2005; Simons *et al*, 2005), suggesting that the involvement of IFT particle components in PCP may be mediated by a mechanism that involves protein–protein interactions identified in our studies (Figure 8). If this is the case, Inversin as well as proteins that mediate its binding to the IFT particle should interact

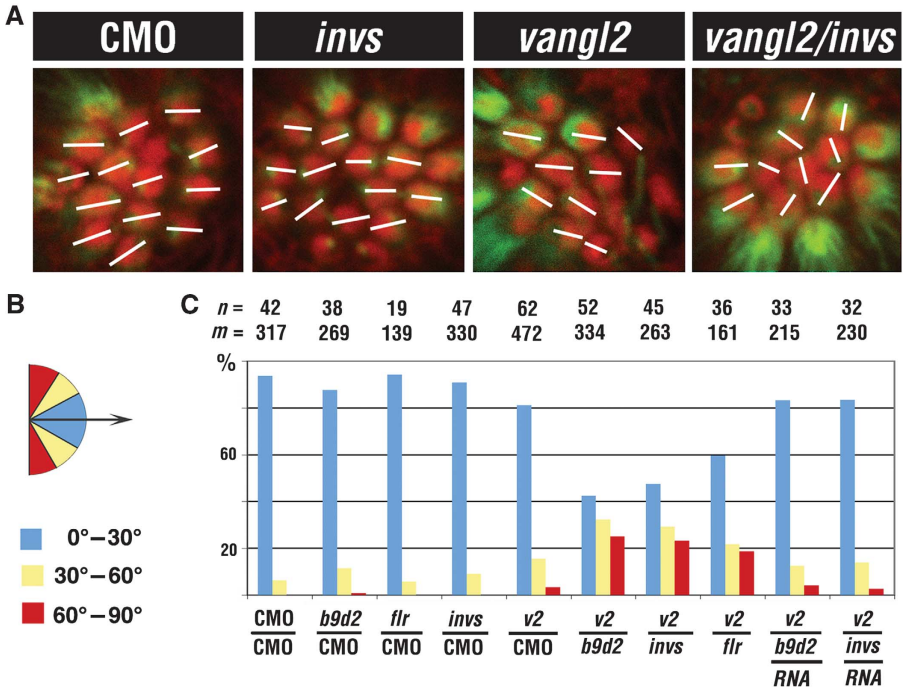

Figure 7 *invs* and *b9d2* contribute to the formation of planar cell polarity in mechanosensory epithelia. (**A**) Confocal images of the L1 neuromast at 4 d.p.f. in whole embryos stained with anti-acetylated-α-tubulin antibodies (green) and phalloidin (red). (**B**) The deviation of hair cell orientation from a common axis (arrow) is assigned to three categories and colour coded as follows: blue, deviation of 1–30°; yellow, 30–60°; red, 60–90°. (**C**) Percent frequencies of misoriented hair cells in single and double morphants in each of three categories. Morpholinos are specified below each set of bars. RNA is *b9d2* or *invs* transcript co-injected with *b9d2* or *invs* morpholino, respectively. *n*, the number of L1 neuromasts investigated. *m*, the number of hair cells. CMO, control morpholino.

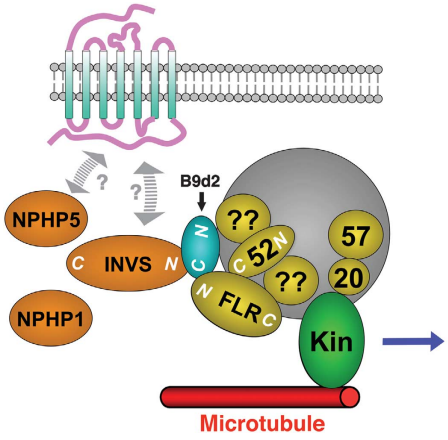

Figure 8 A model of binding interactions. The N-terminal region of Fleer binds the C-termini of Ift52 and B9d2. The C-terminus of B9d2 (depicted in blue) also binds the N-terminal region of Inversin (Nephrocystin 2). Our initial yeast two-hybrid data suggest that the interactions of B9d2 and Fleer with the IFT particle may also involve other IFT proteins (indicated by question marks). Based on prior studies, other Nephrocystins may also complex with Inversin, although it is not clear whether these interactions are direct (Olbrich *et al*, 2003; Otto *et al*, 2003; Mollet *et al*, 2005). The binding interactions between the IFT particle, MKS proteins, and Nephrocystins may take place at the basal body only, or along the ciliary shaft. We also depict known interactions of the kif 3 motor (here 'kin') with the IFT particle as published before (Baker *et al*, 2003; Krock and Perkins, 2008).

genetically with Vangl. Tests of *b9d2*, *invs*, or *vangl2* during convergent extension did not reveal obvious genetic interactions (data not shown). We thus investigated whether *invs*, *b9d2*, and *flr* interact genetically with *vangl2* in the formation of PCP in the zebrafish L1 neuromast. We preformed single and double knockdowns of *vangl2*, *invs*, *b9d2*, or *flr*, and quantitated the presence of misoriented hair cells. We found that planar polarity defects are much more frequent in double morphants, compared with animals treated with single morpholinos (data from four independent tests; Figure 7), and are rescued by mRNA co-injection (Figure 7C). These observations further support the idea that B9d2 and Inversin mediate the interactions of the IFT particle with ciliary membrane proteins, and suggest a mechanism likely to account for PCP defects in Ift88 mutant mice (Jones *et al*, 2008).

Discussion

Although numerous Nephrocystins and MKS proteins have been characterized, the molecular mechanisms that mediate their involvement in ciliogenesis remain unknown. Our data suggest that B9d2, a protein closely structurally and functionally related to MKS protein 1, directly binds IFT particle components. At the same time, B9d2 binds one of the Nephrocystins, Inversin. To our knowledge, for the first time our data provide evidence that Nephrocystins and MKS proteins physically interact with each other and with the IFT machinery. These findings support a model that MKS proteins and Nephrocystins function to facilitate ciliary transport (Figure 8). A malfunction of this transport mechanism is likely to result in an abnormal localization of nonstructural ciliary cargos, such as transmembrane receptors. In addition, our data suggest a mechanism that accounts for the involvement of cilia in PCP.

Inversin and B9d2 proteins are likely to form complexes

Both Inversin and B9d2 proteins are involved in multiple binding interactions. Based on immunoprecipitation studies, Nephrocystins 1 through 4 appear to form a complex (Olbrich *et al*, 2003; Otto *et al*, 2003; Mollet *et al*, 2005). In addition, Inversin has been reported to directly bind two core regulators of PCP pathway, Prickle, and Van Gogh (see below). Similarly, B9d2 also appears to interact closely with other proteins. It is one of three polypeptides that feature the B9 domain. The other two are B9d1 and MKS1. All three proteins function in cilia, and their subcellular localizations are co-dependant. Finally, in double mutants with nematode Nephrocystins, defects in all three genes that encode B9 domain proteins produce very similar ciliary abnormalities (Williams *et al*, 2008; Bialas *et al*, 2009). These findings suggest that B9 domain proteins may also form a complex. It is thus probable that B9 domain proteins as well as Nephrocystins are involved in multiple parallel interactions with the IFT particle. This possibility is supported by the results of our initial yeast two-hybrid tests, suggesting that B9d2 binds Ift88.

A role in ciliary cargo transport

Our data indicate that Inversin and B9d2 function in the transport of ciliary proteins, opsins in particular. Knockdowns of *inversin*, *b9d2*, and at least one other nephrocystin, *nphp5*, slow down the transport of opsin-GFP fusion polypeptide. How do Nephrocystins and MKS proteins mediate opsin transport? Two general scenarios are possible. First, Inversin/B9d2 can function on the 'cargo side' of the IFT transport, and facilitate, directly or indirectly, cargo interaction with the IFT particle. Alternatively, these proteins could function on the 'motor side' of IFT transport, and affect kinesin function. This possibility is suggested by a *C. elegans* model of IFT in which *fleer* homologue, *dyf-1*, affects the binding of the homodimeric Osm-3 kinesin to both the IFT particle and ciliary microtubules (Ou *et al*, 2005). Potential regulators of motor function are likely to travel with the IFT particle. The Fleer protein does so but nematode Nephrocystins and B9 domain proteins, including the MKS1 homologue, localize to basal bodies and are not detected in the ciliary shaft (Williams *et al*, 2008; Bialas *et al*, 2009). These proteins could interact with IFT machinery transiently only at the basal body. Such transient interactions could affect kinesin function, or, more likely, mediate the loading of cargo onto IFT particles. The subsequent interaction of the IFT particle with its cargo in the ciliary axoneme could be maintained by a separate mechanism.

The cargo specificity of Inversin function

Proteins that are essential for the formation of ciliary cytoskeleton, such as tubulin and radial spoke components, are thought to be a cargo of the IFT (Qin *et al*, 2004; reviewed in Silverman and Leroux, 2009). These proteins appear, however, to be transported properly in *inversin* mutants. This conclusion rests on observations that cilia are morphologically intact in inversin-deficient animals. Thus, phenotypic analysis of the *inversion of embryo turning* (*inv*) mutant mouse, in which the *inversin* open reading frame is nearly completely absent, revealed normal structure and motility of cilia (Morgan *et al*, 1998; Watanabe *et al*, 2003; Phillips *et al*, 2004). Likewise, *inversin* knockdowns in zebrafish do not appear to affect cilia morphology (Otto *et al*, 2003). Finally, double knockdowns of *invs* and *b9d2* corroborate this conclusion (this work). Thus, inversin function appears to be dispensable for the transport of essential structural components of ciliary cytoskeleton, and yet it is required for the proper transport of opsin. This suggests that Inversin functions in the transport of a subset of ciliary cargos. Similar conclusion appears to be valid for *nphp5*.

In contrast to Inversin, the association of B9d2 with the IFT particle is more intimate, as double morphants of *b9d2* and *fleer*, an IFT particle component, do cause a shortening of cilia. Both zebrafish and mouse B9d2 localize to the ciliary shaft, and the mouse gene appears to be ubiquitously expressed (this work and Town *et al*, 2008). It is therefore likely that in addition to its interactions with Inversin, B9d2 contributes to the function of the IFT particle in a more general way. This function may, however, vary in different classes of cilia, as we do not observe a mutant phenotype in the kinocilia of *b9d2/fleer* double knockdown embryos (Figure 5D).

A mechanism for degeneration of sensory neurons

Mutations in Nephrocystins (NPHP genes) are associated with defects of vision, olfaction, and, less frequently, hearing. NPHP-associated vision loss is caused by photoreceptor degeneration (reviewed in Hildebrandt *et al*, 2009). Its penetrance varies from $<10\%$, for mutations in the NPHP1 locus for example, to 100% for NPHP6 (reviewed in Hildebrandt *et al*, 2009; Salomon *et al*, 2009). Similarly, olfactory defects have been reported in both human and mouse carriers of hypomorphic NPHP6 mutations (McEwen *et al*, 2007). Finally, genetic lesions in NPHP4 are in some cases associated with hearing loss (Hoefele *et al*, 2005; Mistry *et al*, 2007). The molecular basis of these abnormalities has not been clear so far. Photoreceptor degeneration, for example, could be associated with a number of structural defects in the outer segment or at the base of the connecting cilium. Our studies provide evidence that Nephrocystins and MKS proteins facilitate the transport of ciliary cargo. Consequently, cargo mislocalization is likely to cause degeneration. This possibility is particularly obvious in the case of opsin, which, when mislocalized, is strongly cytotoxic (reviewed in Sung and Tai, 2000; Tan *et al*, 2001; Tsujikawa and Malicki, 2004; Deretic, 2006). This model of degeneration is also supported by studies demonstrating that ciliary G proteins are mislocalized in NPHP6 mutant mice, although the overall ciliary structure remains intact (McEwen *et al*, 2007).

The involvement of IFT proteins in PCP

An interesting study reported that in mouse *polaris/ift88* and *kif3a* mutants, the polarity of hair cells is disrupted in the plane of epithelium, revealing a role for IFT proteins in PCP (Jones *et al*, 2008). Mouse *ift88* mutations do not affect the distribution of planar polarity proteins at apical cell junctions but do affect the planar orientation of apical features, such as the stereociliary bundle. The molecular basis of this function remains, however, unknown. Our data suggest that the role of IFT proteins in PCP is mediated via the ciliary Inversin and Vangl. In support of that, the cytoplasmic tail of Vangl binds to Inversin/Diego, and the Vangl protein has been reported to localize to cilia (Das *et al*, 2004; Ross *et al*, 2005; Simons *et al*, 2005). Functional data are also in agreement with this model:

vangl or *inversin* loss of function cause defects in the convergent extension, a vertebrate model of PCP (Jessen *et al*, 2002; Simons *et al*, 2005). As most IFT proteins are found predominantly at basal bodies and in cilia (e.g., Tsujikawa and Malicki, 2004; Omori *et al*, 2008), Inversin interaction with the IFT particle is likely to take place in the ciliary compartment or at the base of cilia. This mechanism requires further investigation.

Materials and methods

Animals

Zebrafish strains were maintained in standard laboratory conditions in accordance with the guidelines of Tufts University animal care committee.

Yeast two-hybrid analysis

For yeast two-hybrid screening, full-length human *Fleer* (*TTC30B*) cDNA was cloned into the pGBKT7 vector as a bait and used to screen a 17-day mouse embryo cDNA library (Clontech) according to the manufacturer's instructions for Matchmaker System 3 (Clontech). To perform binding tests between Fleer, B9d2 and IFT proteins, *b9d2* and IFT genes were cloned into the pGADT7 vector and transformed along with Fleer bait vector into the AH109 yeast strain. Interactions were identified based on the ability of transformants to grow on His (−), Ade (−) medium. To test interactions between B9d2 and Nephrocystins, Gateway PDEST22 prey vector (for B9D2) and PDEST32 bait vector (for Nephrocystins) were used (Invitrogen). Interactions were tested in the AH109 strain as above. We confirmed all interaction by switching prey and bait vectors.

GST pull-down experiments

To make GST fusion constructs, we cloned B9d2 into PGEX-4T-1 vector (Amersham) and IFT52 into pETG-30A Gateway destination vector (A. Geerlof, EMBL). To make MBP fusion constructs, we cloned the N-terminal human *fleer* fragment (1–364 aa) into the pmal-c2x vector (New England Biolabs), and the N-term Inversin fragment (1–553 aa) into the pETG-41A Gateway destination vector (A. Geerlof, EMBL). MBP fusion proteins were expressed in *Escherichia coli* BL21, and purified using Amylose Resin according to the manufacturer's instructions (New England Biolabs). GST pull-down experiments were performed as described previously (Omori *et al*, 2008). For double pull-down assay, full-length Inversin, Fleer and B9d2 were tagged with MBP, His and GST, respectively, and purified from *E. coli* BL21. To perform pull downs, all three fusion proteins were combined with Amylose resin beads. Pull-down products were detected by western blotting with the following antibodies: anti-His (GE Healthcare Life Sciences), anti-GST (Santa Cruz, SC-459), and anti-MBP (New England Biolabs, E8030S).

Morpholino knockdown

Morpholino knockdown experiments were performed as described previously (Omori *et al*, 2008). Most morpholinos applied in our studies were used in previous publications. The sources, sequences, and concentrations of morpholinos used are listed in Supplementary Table S1. In genetic interaction studies, for single gene knockdowns, gene-targeted morpholinos were mixed with a control morpholino so that the total morpholino concentration was the same as that used for double knockdowns.

Immunohistochemistry and in situ hybridization

Antibody staining was performed using standard protocols (Avanesov and Malicki, 2004). The following primary antibodies and dilutions were used: mouse anti-acetylated-α-tubulin (1:500, Sigma Inc.); rabbit anti-GFP (1:300, Clontech); and mouse anti-opsin (Zpr-3, 1:500, Zebrafish International Resource Center). The staining of cilia was performed as previously (Omori and Malicki, 2006). Alexa Fluor® 546 phalloidin (Invitrogen) was used to visualize hair cells in lateral line neuromasts, and to counterstain olfactory placodes. To perform *in situ* hybridization on *lefty1* and *lefty2* genes, I.M.A.G.E clones were purchased from Open Biosystems/Thermo Fisher Scientific. Probe preparation and hybridization were carried out using standard protocols (Avanesov and Malicki, 2004).

Morphometric analysis

For measurements of olfactory cilia, the surface of the olfactory pit was subdivided in a standardized way into five sectors on confocal images of whole embryos. Measurements were performed using Adobe Photoshop Software (Adobe) and the average was calculated for each section. To evaluate neural tube cilia, we measured the length of all cilia in a constant size area selected on images of zebrafish posterior neural tube collected from whole embryos. The average length was calculated for each animal. To evaluate the differentiation of photoreceptors, we measured the length of inner segment (n) from the pigmented epithelium to the outer limiting membrane, and the length of photoreceptor cell bodies (m) from the pigmented epithelium to the outer plexiform layer. The n/m ratio was used to evaluate the degree of differentiation.

Protein localization in kinocilia

Full-length human *Inversin*, zebrafish *elipsa*, and *EGFP* genes were cloned into the Gateway pDONR221 entry vector (Invitrogen). To generate overexpression constructs, these vectors were combined with a 5′ heat-shock promoter entry vector (p5E-*hsp70l*), a 3′ GFP entry vector (p3E-EGFPpA, or p3E-polyA for GFP only), and a destination vector (pDestTol2pA2) in a single Gateway recombination reaction as described (Kwan *et al*, 2007). The resulting constructs were injected into embryos at the one-cell stage using standard protocols (Avanesov and Malicki, 2004). As EGFP alone is expressed more efficiently, compared with EGFP fusion proteins (Supplementary Figure S7B), the following concentrations of DNA were injected: 5 ng/μl for EGFP, 15 ng/μl for INVS-EGFP, and 20 ng/μl for Eli-EGFP. Embryos were heat shocked at 37°C for 1 h at 28 h.p.f. and fixed at 30 h.p.f. Expression in otic vesicle hair cells was visualized via double staining of whole embryos with anti-GFP and anti-acetylated-α-tubulin antibodies. Signal intensity in the cell body was the highest for hair cells originating from embryos expressing EGFP only, although these animals received the lowest DNA concentration (Supplementary Figure S7B).

To quantitate GFP expression in cilia, embryos were immobilized in 1% low melting point agarose and imaged using ×63 water dipping lens on a Leica TCS-SP2 scope. *Z*-stacks of confocal images encompassing individual hair cells or small groups of GFP-expressing hair cells were collected and projected on a single plane. Hair cells were identified based on the presence of acetylated-α-tubulin staining. Following the separation of RGB images into single channels, ImageJ software was used to calculate mean signal intensity along the entire length of each cilium. In parallel, we measured mean signal intensity in the cell body along a constant length line drawn as a basal extension of the cilium. To compensate for variation in GFP expression level in different hair cells, and for different expression constructs, signal intensity in the cilium was expressed as a ratio of mean signal intensity in the ciliary shaft to mean signal intensity in the cell body.

To visualize the localization of B9D2 in cilia, GFP and GFP-*B9D2* genes were cloned into the pXT7 vector, and used to generate RNA as described (Omori and Malicki, 2006). The *GFP* (200 ng/μl), *GFP-B9D2* (100 ng/μl), *GFP-centrin* (100 ng/μl), or *GFP-elipsa* (100 ng/μl) mRNAs were injected together with anti-*b9d2* MO (for *GFP* and *GFP-B9D2*) or a control morpholino (for *GFP-Elipsa* and *GFP-Centrin*) at the one-cell stage. Embryos were fixed at 24 h.p.f. and double immunostained and imaged as above. GFP signal intensity in cilia was evaluated as above.

Analysis of Opsin and Peripherin/Rds transport

To generate a GFP-rod opsin fusion, we synthesized cDNA fragment encoding the 44 C-terminal amino acids of the Xenopus rod opsin using commercial services (Integrated DNA Technologies, IDT) and inserted it into the Gateway entry vector pDONRp2rp3 (Invitrogen, Inc.). We recombined the resulting vector with p5E-hsp70, pME-EGFP no stop, and pDestTol2PA2 in a multisite Gateway reaction (Kwan *et al*, 2007). To generate the Peripherin-GFP construct, we purchased the full-length human Peripherin2 cDNA from Open-Biosystems, and inserted it into the Gateway entry vector pDONR221 (Invitrogen). The resulting clone was combined with p5E-hsp70, p3E-EGFP, and a destination vector as described above for opsin. The GFP fusion constructs were injected into zebrafish embryos at the one-cell stage along with either control or gene-targeted Morpholinos. Embryos were incubated with 1-phenyl-2-thiourea (PTU) and heated shocked at 72 h.p.f. for 30 min at 37°C. They were fixed 4, 9, and 24 h after heat shock, and cryosectioned

using standard protocols. Sections were counterstained with Alexa-546 Phalloidin and imaged using a Leica TCS-SP2 confocal microscope.

GFP signal intensity in photoreceptor cell bodies was measured in the green channel using the ImageJ software. In each photoreceptor cell, we measured the maximum green pixel value at 25, 50, and 75% of the cell body length. These measurements were subsequently averaged for each cell.

Scoring of neuromast orientation

For each hair cell, we measured the angle between the line connecting the kinocilium with the centre of its apical surface, and another line drawn in parallel to anteroposterior body axis. Based on these measurements, we classified all hair cells into three categories: parallel (0°–30°), oblique (30°–60°), and perpendicular (60°–90°).

Supplementary data

Supplementary data are available at *The EMBO Journal* Online (http://www.embojournal.org).

Acknowledgements

We are thankful to Drs Avidor-Reiss, Solnica-Krezel, Avanesov, and Gupta for comments on earlier versions of this work. We also thank Friedhelm Hildebrandt, Joseph Besharse, Iain Drummond, Chi-Bin Chien, Maureen Barr, Diane Sepich, Arie Geerlof, Nico Katsanis, Carsten Janke, and Ching-Hwa Sung for reagents and/or helpful discussions. Peter Kovach assisted us with electron microscopy. This work was supported by EY018176 and EY016859 R01 awards to JM.

Author contributions: JM and CZ conceived and designed the experiments included in this manuscript. CZ performed the experiments.

Conflict of interest

The authors declare that they have no conflict of interest.

References

Abd-El-Barr MM, Sykoudis K, Andrabi S, Eichers ER, Pennesi ME, Tan PL, Wilson JH, Katsanis N, Lupski JR, Wu SM (2007) Impaired photoreceptor protein transport and synaptic transmission in a mouse model of Bardet-Biedl syndrome. *Vision Res* **47:** 3394–3407

Adams NA, Awadein A, Toma HS (2007) The retinal ciliopathies. *Ophthalmic Genet* **28:** 113–125

Avanesov A, Malicki J (2004) Approaches to study neurogenesis in the zebrafish retina. *Methods Cell Biol* **76:** 333–384

Baker SA, Freeman K, Luby-Phelps K, Pazour GJ, Besharse JC (2003) IFT20 links kinesin II with a mammalian intraflagellar transport complex that is conserved in motile flagella and sensory cilia. *J Biol Chem* **278:** 34211–34218

Bialas NJ, Inglis PN, Li C, Robinson JF, Parker JD, Healey MP, Davis EE, Inglis CD, Toivonen T, Cottell DC, Blacque OE, Quarmby LM, Katsanis N, Leroux MR (2009) Functional interactions between the ciliopathy-associated Meckel syndrome 1 (MKS1) protein and two novel MKS1-related (MKSR) proteins. *J Cell Sci* **122** (Part 5)**:** 611–624

Bisgrove BW, Essner JJ, Yost HJ (1999) Regulation of midline development by antagonism of lefty and nodal signaling. *Development* **126:** 3253–3262

Das G, Jenny A, Klein TJ, Eaton S, Mlodzik M (2004) Diego interacts with Prickle and Strabismus/Van Gogh to localize planar cell polarity complexes. *Development* **131:** 4467–4476

Deretic D (2006) A role for rhodopsin in a signal transduction cascade that regulates membrane trafficking and photoreceptor polarity. *Vision Res* **46:** 4427–4433

Doerre G, Malicki J (2002) Genetic analysis of photoreceptor cell development in the zebrafish retina. *Mech Dev* **110:** 125–138

Fan ZC, Behal RH, Geimer S, Wang Z, Williamson SM, Zhang H, Cole DG, Qin H (2010) Chlamydomonas IFT70/CrDYF-1 is a core component of IFT particle complex B and is required for flagellar assembly. *Mol Biol Cell* **21:** 2696–2706

Hengl T, Kaneko H, Dauner K, Vocke K, Frings S, Mohrlen F (2010) Molecular components of signal amplification in olfactory sensory cilia. *Proc Natl Acad Sci USA* **107:** 6052–6057

Hildebrandt F, Attanasio M, Otto E (2009) Nephronophthisis: disease mechanisms of a ciliopathy. *J Am Soc Nephrol* **20:** 23–35

Hoefele J, Sudbrak R, Reinhardt R, Lehrack S, Hennig S, Imm A, Muerb U, Utsch B, Attanasio M, O'Toole JF, Otto E, Hildebrandt F (2005) Mutational analysis of the NPHP4 gene in 250 patients with nephronophthisis. *Hum Mutat* **25:** 411

Jenkins PM, McEwen DP, Martens JR (2009) Olfactory cilia: linking sensory cilia function and human disease. *Chem Senses* **34:** 451–464

Jessen JR, Topczewski J, Bingham S, Sepich DS, Marlow F, Chandrasekhar A, Solnica-Krezel L (2002) Zebrafish trilobite identifies new roles for Strabismus in gastrulation and neuronal movements. *Nat Cell Biol* **4:** 610–615

Jin H, White SR, Shida T, Schulz S, Aguiar M, Gygi SP, Bazan JF, Nachury MV (2010) The conserved Bardet-Biedl syndrome proteins assemble a coat that traffics membrane proteins to cilia. *Cell* **141:** 1208–1219

Jones C, Roper VC, Foucher I, Qian D, Banizs B, Petit C, Yoder BK, Chen P (2008) Ciliary proteins link basal body polarization to planar cell polarity regulation. *Nat Genet* **40:** 69–77

Kennedy B, Malicki J (2009) What drives cell morphogenesis: a look inside the vertebrate photoreceptor. *Dev Dyn* **238:** 2115–2138

Khaddour R, Smith U, Baala L, Martinovic J, Clavering D, Shaffiq R, Ozilou C, Cullinane A, Kyttala M, Shalev S, Audollent S, d'Humieres C, Kadhom N, Esculpavit C, Viot G, Boone C, Oien C, Encha-Razavi F, Batman PA, Bennett CP *et al* (2007) Spectrum of MKS1 and MKS3 mutations in Meckel syndrome: a genotype-phenotype correlation. Mutation in brief #960. Online. *Hum Mutat* **28:** 523–524

Krock BL, Perkins BD (2008) The intraflagellar transport protein IFT57 is required for cilia maintenance and regulates IFT-particle-kinesin-II dissociation in vertebrate photoreceptors. *J Cell Sci* **121** (Part 11)**:** 1907–1915

Kwan KM, Fujimoto E, Grabher C, Mangum BD, Hardy ME, Campbell DS, Parant JM, Yost HJ, Kanki JP, Chien CB (2007) The Tol2kit: a multisite gateway-based construction kit for Tol2 transposon transgenesis constructs. *Dev Dyn* **236:** 3088–3099

Leitch CC, Zaghloul NA, Davis EE, Stoetzel C, Diaz-Font A, Rix S, Alfadhel M, Lewis RA, Eyaid W, Banin E, Dollfus H, Beales PL, Badano JL, Katsanis N (2008) Hypomorphic mutations in syndromic encephalocele genes are associated with Bardet-Biedl syndrome. *Nat Genet* **40:** 443–448

Marszalek JR, Liu X, Roberts EA, Chui D, Marth JD, Williams DS, Goldstein LS (2000) Genetic evidence for selective transport of opsin and arrestin by kinesin-II in mammalian photoreceptors. *Cell* **102:** 175–187

McEwen DP, Koenekoop RK, Khanna H, Jenkins PM, Lopez I, Swaroop A, Martens JR (2007) Hypomorphic CEP290/NPHP6 mutations result in anosmia caused by the selective loss of G proteins in cilia of olfactory sensory neurons. *Proc Natl Acad Sci USA* **104:** 15917–15922

Mistry K, Ireland JH, Ng RC, Henderson JM, Pollak MR (2007) Novel mutations in NPHP4 in a consanguineous family with histological findings of focal segmental glomerulosclerosis. *Am J Kidney Dis* **50:** 855–864

Mollet G, Silbermann F, Delous M, Salomon R, Antignac C, Saunier S (2005) Characterization of the nephrocystin/nephrocystin-4 complex and subcellular localization of nephrocystin-4 to primary cilia and centrosomes. *Hum Mol Genet* **14:** 645–656

Morgan D, Eley L, Sayer J, Strachan T, Yates LM, Craighead AS, Goodship JA (2002a) Expression analyses and interaction with the anaphase promoting complex protein Apc2 suggest a role for inversin in primary cilia and involvement in the cell cycle. *Hum Mol Genet* **11:** 3345–3350

Morgan D, Goodship J, Essner JJ, Vogan KJ, Turnpenny L, Yost HJ, Tabin CJ, Strachan T (2002b) The left-right determinant inversin has highly conserved ankyrin repeat and IQ domains and interacts with calmodulin. *Hum Genet* **110:** 377–384

Morgan D, Turnpenny L, Goodship J, Dai W, Majumder K, Matthews L, Gardner A, Schuster G, Vien L, Harrison W, Elder FF, Penman-

Splitt M, Overbeek P, Strachan T (1998) Inversin, a novel gene in the vertebrate left-right axis pathway, is partially deleted in the inv mouse. *Nat Genet* **20:** 149–156

Murcia NS, Richards WG, Yoder BK, Mucenski ML, Dunlap JR, Woychik RP (2000) The Oak Ridge Polycystic Kidney (orpk) disease gene is required for left-right axis determination. *Development* **127:** 2347–2355

Nachury MV, Loktev AV, Zhang Q, Westlake CJ, Peranen J, Merdes A, Slusarski DC, Scheller RH, Bazan JF, Sheffield VC, Jackson PK (2007) A core complex of BBS proteins cooperates with the GTPase Rab8 to promote ciliary membrane biogenesis. *Cell* **129:** 1201–1213

Nurnberger J, Bacallao RL, Phillips CL (2002) Inversin forms a complex with catenins and N-cadherin in polarized epithelial cells. *Mol Biol Cell* **13:** 3096–3106

O'Toole JF, Otto EA, Frishberg Y, Hildebrandt F (2006) Retinitis pigmentosa and renal failure in a patient with mutations in INVS. *Nephrol Dial Transplant* **21:** 1989–1991

Olbrich H, Fliegauf M, Hoefele J, Kispert A, Otto E, Volz A, Wolf MT, Sasmaz G, Trauer U, Reinhardt R, Sudbrak R, Antignac C, Gretz N, Walz G, Schermer B, Benzing T, Hildebrandt F, Omran H (2003) Mutations in a novel gene, NPHP3, cause adolescent nephronophthisis, tapeto-retinal degeneration and hepatic fibrosis. *Nat Genet* **34:** 455–459

Omori Y, Malicki J (2006) oko meduzy and related crumbs genes are determinants of apical cell features in the vertebrate embryo. *Curr Biol* **16:** 945–957

Omori Y, Zhao C, Saras A, Mukhopadhyay S, Kim W, Furukawa T, Sengupta P, Veraksa A, Malicki J (2008) Elipsa is an early determinant of ciliogenesis that links the IFT particle to membrane-associated small GTPase Rab8. *Nat Cell Bio* **10:** 437–444

Otto EA, Schermer B, Obara T, O'Toole JF, Hiller KS, Mueller AM, Ruf RG, Hoefele J, Beekmann F, Landau D, Foreman JW, Goodship JA, Strachan T, Kispert A, Wolf MT, Gagnadoux MF, Nivet H, Antignac C, Walz G, Drummond IA *et al* (2003) Mutations in INVS encoding inversin cause nephronophthisis type 2, linking renal cystic disease to the function of primary cilia and left-right axis determination. *Nat Genet* **34:** 413–420

Ou G, Blacque OE, Snow JJ, Leroux MR, Scholey JM (2005) Functional coordination of intraflagellar transport motors. *Nature* **436:** 583–587

Pathak N, Obara T, Mangos S, Liu Y, Drummond IA (2007) The zebrafish fleer gene encodes an essential regulator of cilia tubulin polyglutamylation. *Mol Biol Cell* **18:** 4353–4364

Pedersen LB, Rosenbaum JL (2008) Chapter Two Intraflagellar Transport (IFT) role in ciliary assembly, resorption and signalling. *Curr Top Dev Biol* **85:** 23–61

Phillips CL, Miller KJ, Filson AJ, Nurnberger J, Clendenon JL, Cook GW, Dunn KW, Overbeek PA, Gattone II VH, Bacallao RL (2004) Renal cysts of inv/inv mice resemble early infantile nephronophthisis. *J Am Soc Nephrol* **15:** 1744–1755

Pugh E, Lamb T (2000) Phototransduction in vertebrate rods and cones. In *Handbook of Biological Physics*, Stavenga DG, de Grip WJ, Pugh Jr EN (eds), Vol. 3, pp 183–255. Elsevier Science B. V.

Qin H, Diener DR, Geimer S, Cole DG, Rosenbaum JL (2004) Intraflagellar transport (IFT) cargo: IFT transports flagellar precursors to the tip and turnover products to the cell body. *J Cell Biol* **164:** 255–266

Rodieck RW (1973) *The Vertebrate Retina. Principles of Structure and Function*. San Francisco, California: W.H. Freeman & Co

Rosenbaum JL, Witman GB (2002) Intraflagellar transport. *Nat Rev Mol Cell Biol* **3:** 813–825

Ross AJ, May-Simera H, Eichers ER, Kai M, Hill J, Jagger DJ, Leitch CC, Chapple JP, Munro PM, Fisher S, Tan PL, Phillips HM, Leroux MR, Henderson DJ, Murdoch JN, Copp AJ, Eliot MM, Lupski JR, Kemp DT, Dollfus H *et al* (2005) Disruption of Bardet-Biedl syndrome ciliary proteins perturbs planar cell polarity in vertebrates. *Nat Genet* **37:** 1135–1140

Salomon R, Saunier S, Niaudet P (2009) Nephronophthisis. *Pediatr Nephrol* **24:** 2333–2344

Seo S, Baye LM, Schulz NP, Beck JS, Zhang Q, Slusarski DC, Sheffield VC (2010) BBS6, BBS10, and BBS12 form a complex with CCT/TRiC family chaperonins and mediate BBSome assembly. *Proc Natl Acad Sci USA* **107:** 1488–1493

Silverman MA, Leroux MR (2009) Intraflagellar transport and the generation of dynamic, structurally and functionally diverse cilia. *Trends Cell Biol* **19:** 306–316

Simons M, Gloy J, Ganner A, Bullerkotte A, Bashkurov M, Kronig C, Schermer B, Benzing T, Cabello OA, Jenny A, Mlodzik M, Polok B, Driever W, Obara T, Walz G (2005) Inversin, the gene product mutated in nephronophthisis type II, functions as a molecular switch between Wnt signaling pathways. *Nat Genet* **37:** 537–543

Sun Z, Amsterdam A, Pazour GJ, Cole DG, Miller MS, Hopkins N (2004) A genetic screen in zebrafish identifies cilia genes as a principal cause of cystic kidney. *Development* **131:** 4085–4093

Sung CH, Tai AW (2000) Rhodopsin trafficking and its role in retinal dystrophies. *Int Rev Cytol* **195:** 215–267

Tam BM, Moritz OL, Hurd LB, Papermaster DS (2000) Identification of an outer segment targeting signal in the COOH terminus of rhodopsin using transgenic Xenopus laevis. *J Cell Biol* **151:** 1369–1380

Tam BM, Moritz OL, Papermaster DS (2004) The C terminus of peripherin/rds participates in rod outer segment targeting and alignment of disk incisures. *Mol Biol Cell* **15:** 2027–2037

Tan E, Wang Q, Quiambao AB, Xu X, Qtaishat NM, Peachey NS, Lem J, Fliesler SJ, Pepperberg DR, Naash MI, Al-Ubaidi MR (2001) The relationship between opsin overexpression and photoreceptor degeneration. *Invest Ophthalmol Vis Sci* **42:** 589–600

Town T, Breunig JJ, Sarkisian MR, Spilianakis C, Ayoub AE, Liu X, Ferrandino AF, Gallagher AR, Li MO, Rakic P, Flavell RA (2008) The stumpy gene is required for mammalian ciliogenesis. *Proc Natl Acad Sci USA* **105:** 2853–2858

Tsujikawa M, Malicki J (2004) Intraflagellar transport genes are essential for differentiation and survival of vertebrate sensory neurons. *Neuron* **42:** 703–716

Valente EM, Logan CV, Mougou-Zerelli S, Lee JH, Silhavy JL, Brancati F, Iannicelli M, Travaglini L, Romani S, Illi B, Adams M, Szymanska K, Mazzotta A, Lee JE, Tolentino JC, Swistun D, Salpietro CD, Fede C, Gabriel S, Russ C *et al* (2010) Mutations in TMEM216 perturb ciliogenesis and cause Joubert, Meckel and related syndromes. *Nat Genet* **42:** 619–625

Watanabe D, Saijoh Y, Nonaka S, Sasaki G, Ikawa Y, Yokoyama T, Hamada H (2003) The left-right determinant Inversin is a component of node monocilia and other 9 + 0 cilia. *Development* **130:** 1725–1734

Weatherbee SD, Niswander LA, Anderson KV (2009) A mouse model for Meckel syndrome reveals Mks1 is required for ciliogenesis and Hedgehog signaling. *Hum Mol Genet* **18:** 4565–4575

Williams CL, Winkelbauer ME, Schafer JC, Michaud EJ, Yoder BK (2008) Functional redundancy of the B9 proteins and nephrocystins in *Caenorhabditis elegans* ciliogenesis. *Mol Biol Cell* **19:** 2154–2168

Zhao C, Malicki J (2007) Genetic defects of pronephric cilia in zebrafish. *Mech Dev* **124:** 605–616

Zhao Y, Hong DH, Pawlyk B, Yue G, Adamian M, Grynberg M, Godzik A, Li T (2003) The retinitis pigmentosa GTPase regulator (RPGR)-interacting protein: subserving RPGR function and participating in disk morphogenesis. *Proc Natl Acad Sci USA* **100:** 3965–3970

